On Subgrid Models and Filter Operations in Large Eddy Simulations

P. J. MASON AND A. R. BROWN

Meteorological Office, Bracknell, Berkshire, United Kingdom

(Manuscript received 29 September 1997, in final form 16 July 1998)

ABSTRACT

Large eddy simulations use a subgrid model, which is characterized by a length scale that is often related to the scale of the computational mesh by a numerical constant, C_s. Mason and Callen argued that this subgrid model and its length scale define and impose the filter operation of the simulation. They saw C_s as a measure of numerical accuracy. Others have sought to link the filter operation to the computational mesh and have viewed C_s as needing determination for correct implementation. Here tests with a high resolution of $224 \times 224 \times 200$ grid points are found to confirm Mason and Callen's view. These simulations are also used together with lower-resolution simulations to illustrate the degree of convergence achieved. Some erroneous features of the simulations are identified through this test.

For the case of buoyant convection, the buoyancy dependence of the subgrid model is further examined. Most available subgrid models allow for buoyancy fluxes changing the level of the subgrid energy but only allow stable buoyancy gradients to modify the subgrid length scale—a reduction in this case. In contrast to most applications, it has been suggested that for a fixed filter operation, the subgrid length scale should always have a buoyancy dependence and should increase, in a finite way, with unstable buoyant transfer. Here an examination of spectral behavior in high-resolution simulations supports such an approach and shows that the model with the buoyancy-dependent length scale is indeed consistent with a fixed filter operation. The more conventional models are shown to have less satisfactory behavior.

1. Introduction

A large eddy simulation (LES) is based on the concept that the Navier–Stokes equations describing a flow have been subject to a filter operation. This operation separates the resolved-scale motions (which will be explicitly represented in the numerical simulation) from the unresolved or subgrid scales (the effects of which will be parameterized by the subgrid model). Strictly, ''subgrid'' would be better described as ''subfilter'' (as no link to a numerical discretization is implied), but the former term is almost universally used and has been adopted here. It is usual to relate the subgrid model to a filter operation but there are distinctly different views between authors on the nature of this relationship and indeed on expected consequences of the filter operation upon the resolved motions. The expected role of the numerical mesh is a related issue also subject to matching differences in views. The purpose of this paper is to use new high-resolution large eddy simulations to test these and other issues concerning the subgrid model.

The simulations considered here are of a convective planetary boundary layer and are of an effectively infinite Reynolds number flow. The direct influence of molecular viscosity on the resolved-scale motions is wholly negligible. This limit of high Reynolds number is the circumstance for which the formal concept of large eddy simulation has been developed and it is the intended circumstance for the arguments of Mason and Callen (1986) to apply. At low and moderate Reynolds numbers there will be a direct influence of molecular viscosity on the resolved motions. The high–Reynolds number subgrid models should not be expected to be correct and, at least in the limit of a tendency toward flow laminarization, will be too dissipative. In such circumstances large eddy simulations have been achieved through the use of so-called dynamic models (e.g., Germano et al. 1991), which adjust the dissipation of the subgrid model so as to avoid any tendency for rate of decrease of turbulence energy with decreasing spectral scale to exceed the inertial subrange value. Such models are fairly unique in their success at low Reynolds numbers. At high Reynolds numbers successful application also seems possible but difficulties remain in matching the dynamic model to high–Reynolds number boundary conditions where, even close to the surface, direct molecular effects are weak or negligible. The present study will focus on the application of subgrid models of the type first proposed by Smagorinsky (1963), but the implications of the results for these dynamic models are also discussed.

Corresponding author address: Dr. Andrew R. Brown, Meteorological Office, Bracknell, Berkshire RG12 2SZ, United Kingdom.
E-mail: arbrown@meto.gov.uk

Unauthenticated | Downloaded 07/25/21 03:39 AM UTC

The Smagorinsky model contains a single basic length scale, λ_0. The analysis of Lilly (1967) allows an estimate to be made of the relationship between this scale and the implied filter scale l_f. This is done by assuming a particular filter shape (often a sharp cut in spectral space) and insisting that the ensemble-averaged dissipation across this filter from resolved to subgrid scales, which is given by the model, should be that expected in an inertial subrange. This consistency in characteristic scale is well based, but the issue of what exact shape or form of filter operation is actually used in the simulation remains. In terms of concept Mason and Callen (1986) noted that the continuous equations for the resolved-scale velocity were only aware of any filter operation through the influence of this subgrid model. The resolved-scale model equations are then simply the Navier–Stokes equations with the molecular viscosity terms replaced by the subgrid model and its derivation of a stress tensor. In these continuous equations it is clear that Mason and Callen must be correct and that the subgrid model alone determines and defines both the scale and form of the filter operation. Further to this, tests with a constant value of eddy viscosity, chosen in value to ensure the same equality of dissipation, give near-identical results to those obtained with the Smagorinsky subgrid model (Mason and Brown 1994). This suggests that the form of the filter imposed by the Smagorinsky model is similar in structure to that effected by a constant viscosity. The work of Muschinski (1996) gives further detail and support to this view.

Recognizing that differences in views would seem unlikely if attention were confined to the continuous equations, it is clear that different views of the consequences of numerical implementation must account for the varied views. The constant C_s is the ratio of the length scale in the Smagorinsky model to a measure of the numerical resolution such as the grid spacing itself. Mason and Callen noted that a numerical simulation with a very large value of C_s (i.e., high resolution in relation to the scale of the filter represented by the subgrid model) must closely approximate the continuous equation solution with the matching value of filter scale. In this limit the resolved-scale motions should have little variance on the grid scale. The resolved motion spectra should show a decay of energy matching that expected from the application of the subgrid model in the continuous case.

Use of large values of C_s is, however, clearly computationally very expensive in terms of effective use of the numerical mesh. As C_s is reduced, the expected filter operation will be represented with less fidelity and finite difference errors will occur as energy increases at the grid scale. The spectra can be expected to decay less rapidly, and for sufficiently small C_s there is a risk of energy building up and the spectra failing to show any decay at short scales. Should the numerical methods used be dissipative, then this behavior will be limited, but the numerical dissipation itself forms part of the subgrid model, and the continuous equations being solved are hard to specify. Mason and Callen suggested that the optimum value of C_s would be one at which finite difference errors were moderate but limited. While this value may show some sensitivity to the numerical methods used, in practice, it is likely to be when the filter scale is roughly equal to the size of the numerical mesh. The analysis of Lilly (1967) suggests that values of C_s of around 0.2 should correspond to this circumstance.

While the view of Mason and Callen has some strong support, many and perhaps a majority, of users of large eddy simulations continue to take a different view. A common one, often implicitly assumed, is to formally consider the numerical mesh itself acting as a filter, and often one with a sharp spectral cut. This approach leads to a view that there is a correct value of C_s corresponding to the resolved-scale spectral slope having the value expected in an inertial subrange at the finest resolved scales. Other values are considered wrong and studies have sought to find this correct value for particular flows or determine it within the flow with so-called dynamic models.

Other modelers adopt an approach based on the work of Leonard (1974), which recast the basic equations by considering an explicit filter operation applied to the nonlinear term in the equations of motion. While this leads to a formally legitimate redefinition of the subgrid stress term, this stress cannot then be directly linked to the Lilly (1967) analysis and much of the dissipation occurs in the explicit filtering. Those with spectral models often use as the explicit filter operation a spectral wavenumber cutoff, which may be restricted to two dimensions (e.g., Moeng and Wyngaard 1988). With this approach the consistency between the explicit filter operation and the length scale and shape of the filter implied by the subgrid term is not clear. In as much as these studies using the Leonard approach seek a spectral slope consistent with the explicit filter, they do not associate the filter with the subgrid term. The Mason and Callen interpretation of such methods would be that both the explicit filter and the subgrid closure *together* define the filter operation (as both lead to dissipation), whether or not they are wholly consistent.

Often there may not be any large practical consequence to the difference between believing the filter to be related to the subgrid model and believing it to be related to the numerical grid, if only because the values of C_s actually used in simulations may not differ very strongly. Nevertheless, the Mason and Callen argument that it should be possible to use arbitrarily large C_s (i.e., arbitrarily high resolution for a given value of λ_0) is crucially different from the more traditional view. There are also concerns that if Mason and Callen are correct, then other simulations that attempt to insist that the numerical grid acts as the filter may have undue finite difference errors and be at risk of erroneous interpretation of the simulated spectra in particular. The overall

Unauthenticated | Downloaded 07/25/21 03:39 AM UTC

interpretation of the simulation of course also remains of concern for best development of the technique.

The aim here is to clarify which viewpoint is indeed consistent with the behavior of the simulations. Suitable tests are easy to conceive but in practice they have been seldom applied, as they require an ability to vary the numerical resolution in the simulations by a significant factor simultaneously in all three directions. This must be achieved at the same time as ensuring that the poorest resolution is adequate. Unless this is the case, the solutions may be quite different for reasons of basic resolution alone and other issues will remain obscure. The present choice of simulating the convective planetary boundary layer was made because it is easy to simulate credibly with moderate resolution and is also a familiar case.

The choice of the convective boundary layer further allows an extension of our objectives to seek to clarify the issues of buoyancy dependence in the subgrid model. This influence should not be directly significant in the flow interior where resolution of a significant inertial subrange is probable, but it does become an issue as the surface is approached. Most subgrid models allow for the influence of buoyancy effects in the energy equation and, hence, in the velocity scale. However, Mason (1989) suggested that a greater buoyancy dependance should occur, with the subgrid model length scale increasing (in a finite way) with an unstable buoyancy gradient. His model was further refined by Brown et al. (1994), based on surface layer observations, to give a still stronger stability dependence. The spectral behavior in the near-surface region of simulations with both types of subgrid model is examined in the present study.

As noted and considered by Mason and Thomson (1992) and Schumann (1995), the Smagorinsky model does, however, neglect the real somewhat stochastic nature of subgrid-scale stresses. These fluctuations in stress induce a backscatter of energy from the subgrid to the resolved scales. Mason and Thomson developed a model to represent this process and their model was extended to include buoyancy effects by Brown et al. (1994). Its use was shown to lead to much improved simulation of the stable atmospheric boundary layer. However, it is not expected to be of much practical significance in flows such as buoyant convection where the main processes should all be well resolved. Some results will be presented to confirm that this is the case.

Finally, the set of simulations provide a very high-resolution simulation of inherent interest, which is enhanced by the further ability to judge evidence for convergence of results with increasing resolution.

2. The large eddy model

A filter operation is applied to the Navier–Stokes equations for a Boussinesq fluid with reference temperature θ_r, and a numerical solution is sought to the following continuous equations for the resolved velocity $(u_1, u_2, u_3) = (u, v, w)$ and potential temperature θ. Einstein summation notation is used:

$$\frac{\partial u_i}{\partial t} + \frac{\partial (u_i u_j)}{\partial x_j} = -\frac{\partial p}{\partial x_i} + \delta_{i3}\left(\frac{g}{\theta_r}\right)(\theta - \theta_r) - \frac{\partial \tau_{ij}}{\partial x_j} - 2\epsilon_{ijk}\Omega_j u_k; \quad (1)$$

$$\frac{\partial u_i}{\partial x_i} = 0; \quad (2)$$

$$\frac{\partial \theta}{\partial t} + \frac{\partial (u_i \theta)}{\partial x_i} = -\frac{\partial H_i}{\partial x_i}. \quad (3)$$

Here p is the dynamic pressure and g is the acceleration due to gravity. The last term is the Coriolis term (at 45°N). While this was included in the present convective boundary layer simulations, its influence is quite negligible. The subgrid stress tensor τ_{ij} and the subgrid heat flux H_i have to be parameterized (see next section). In keeping with the high Reynolds number of the atmospheric boundary layer, the effects of molecular viscosity on the resolved fields are neglected. Mention of density is suppressed (equivalent to choosing units of mass so that the density is unity), so that both energy and stress have units of meters squared per second squared.

The numerical procedure uses a staggered grid and is second-order accurate in space for a mesh with slowly varying vertical spacing. The leapfrog time-marching scheme with the Piacsek and Williams (1970) form of the nonlinear terms ensures conservation of energy and scalar variance. Viscous terms are advanced in time with a simple forward time step for numerical stability. Boundary conditions are periodic in the horizontal directions, with a damping layer (well above the region of interest) below a stress-free rigid lid at the top of the domain. The surface boundary conditions (no slip and imposed heat flux) are applied by assuming local equilibrium between each of the lowest points and the surface (roughness lengths $z_0 = z_{0\theta} = 0.1$ m) and applying Monin–Obukhov similarity at each point.

a. The subgrid model

The model used is the extension of the Smagorinsky (1963) model discussed by Brown et al. (1994), the subgrid terms being specified through

$$\tau_{ij} = -\nu\left(\frac{\partial u_i}{\partial x_j} + \frac{\partial u_j}{\partial x_i}\right) \quad (4)$$

and

$$H_i = -\nu_h \frac{\partial \theta}{\partial x_i}. \quad (5)$$

The eddy viscosity (ν) and diffusivity (ν_h) are given by

Unauthenticated | Downloaded 07/25/21 03:39 AM UTC

$$\nu = \lambda_r^2 S(1 - \mathrm{Rf}_p)^{1/2} = \lambda^2 S f_m(\mathrm{Ri}_p), \quad (6)$$

$$\nu_h = \nu/\mathrm{Pr} = \lambda^2 S f_h(\mathrm{Ri}_p), \quad (7)$$

where

$$S^2 = \frac{1}{2}\left(\frac{\partial u_i}{\partial x_j} + \frac{\partial u_j}{\partial x_i}\right)^2. \quad (8)$$

Here λ_r is a characteristic subgrid length scale, λ is the neutral value of this length scale (see below), Pr is the Prandtl number, Rf_p is the local flux Richardson number (calculated pointwise), and f_m and f_h are functions of the local gradient Richardson number ($\mathrm{Ri}_p = \mathrm{Rf}_p\mathrm{Pr}$). These functions are given in the appendix for ease of reference. Estimates of subgrid energy (E) and scalar variance (E_θ) are made using Eqs. (15) and (16) of Brown et al. (1994).

In the interior of the flow, the basic neutral length scale λ has a constant value, λ_0, which, following Mason and Callen (1986), implies a filter scale, l_f. Near the surface λ must be equal to κz where κ is the von Karman constant, z is the distance from the surface, and a match is achieved through

$$\frac{1}{\lambda^2} = \frac{1}{\lambda_0^2} + \frac{1}{(\kappa z)^2}. \quad (9)$$

The simplest and most conventional extension to include stability effects takes $\lambda_r = \lambda$, which considers only the direct influence of buoyancy on subgrid energy production (Lilly 1962). In contrast, the refined model of Brown et al. (1994), which is used in the present study, specifies f_m and f_h directly, based on observations from the atmospheric surface layer. Near the surface such a form simply ensures the correct Monin–Obukhov behavior, but in the interior it implies the use of a λ_r, which is not equal to λ. The value of λ_r implied by this model can be diagnosed using Eq. (6), and it can be seen to increase above its neutral value in unstable conditions (with an asymptotic value of 1.8λ in free convective conditions) while decreasing to zero at a critical Richardson number (Ri_c) of 0.25 in stable conditions (Fig. 1). The Prandtl number also becomes stability dependent, increasing from 0.44 in the free convective limit, to 0.7 in neutral conditions and 1.0 at $\mathrm{Ri}_p = \mathrm{Ri}_c$. It is noted that the simple fit to observed stability functions either side of $\mathrm{Ri}_p = 0$ gives a discontinuous gradient at $\mathrm{Ri}_p = 0$, but this is thought to be of little consequence.

This stability-dependent subgrid model has been shown to lead to improved results in large eddy simulations of the stable boundary layer (Brown et al. 1994). In convective conditions the revised model seems most likely to have a significant direct impact in the relatively poorly resolved region close to the surface, and changes in this region may then lead to some wider impact. Mason (1989) compared results obtained with a conventional model ($\lambda_r = \lambda$) and with a modified model in which the subgrid length scale increased with increasing instability, although not as strongly as in Brown et al. (1994). The modified model appeared to give better results but was still subject to finite difference errors in the near-surface region, and Mason suggested a still stronger stability dependence. Hence there is good reason to expect that the model of Brown et al. (1994) should perform satisfactorily, but this must be investigated, and the spectral behavior in the near-surface region of simulations using this model will be studied in some detail in the present paper. For comparison, results will also be presented from a simulation using what will be referred to as the ''conventional model''; in fact, this retains the closure of Brown et al. (1994) in stable conditions, but λ_r/λ and Pr are kept at their neutral values in unstable conditions (see Fig. 1) so as to match more closely the behavior of most other subgrid models.

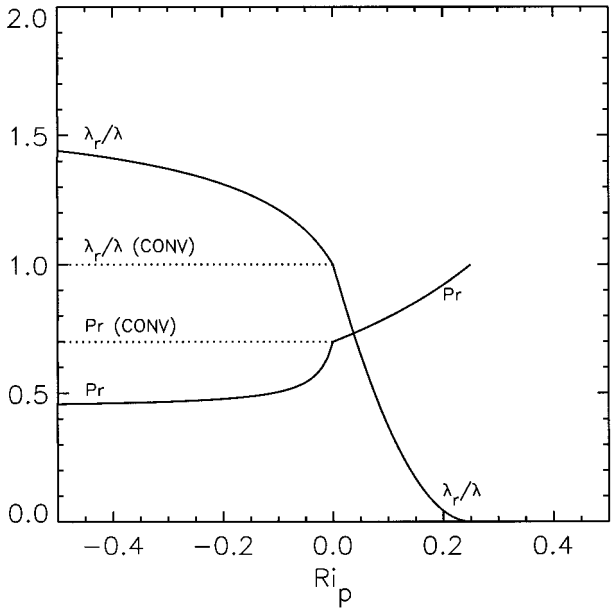

FIG. 1. Ratio of characteristic subgrid length scale (λ_r) to its neutral value (λ), and Prandtl number (Pr), as functions of pointwise Richardson number (Ri_p). Solid lines represent model of Brown et al. (1994); dotted lines, conventional model (see text) in unstable conditions.

b. Simulations performed

Each simulation was initialized with $\theta = \theta_r = 300$ K from the surface up to $z = 1000$ m, with θ then increasing linearly at 0.003 K m^{-1} until the domain top at 3000 m. The wind components were set to zero. A small perturbation (± 0.5 K) was applied to the potential temperature at the lowest model level to initiate turbulence, and a surface heat flux ($\langle w'\theta'\rangle_0$) of 0.06 K m s^{-1} was imposed.

Many of these simulations were originally performed as part of a study to examine the influence of differing mean structures in the inversion region on the modeled entrainment flux. Accordingly, an extra source term was

Unauthenticated | Downloaded 07/25/21 03:39 AM UTC

TABLE 1. Summary of main runs. The naming convention is chosen so that the grid resolution (from A to F) and the value of λ_0 used can be immediately ascertained.

Run	$N_{x,y}$	$\Delta_{x,y}$ (m)	N_z	Δ_z (m)	λ_0 (m)	C_s	Subgrid model	Backscatter
A29	32	125.0	61	50.0	28.8	0.23	STAB	Off
A29_CONV	32	125.0	61	50.0	28.8	0.23	CONV	Off
A14	32	125.0	61	50.0	14.4	0.12	STAB	Off
B14	45	88.9	61	50.0	14.4	0.16	STAB	Off
C14	64	62.5	69	50.0	14.4	0.23	STAB	Off
D14	90	44.4	100	20.0	14.4	0.32	STAB	Off
E14	128	31.3	100	20.0	14.4	0.46	STAB	Off
F14	224	17.9	200	10.0	14.4	0.81	STAB	Off
C14_BIG	224	62.5	69	50.0	14.4	0.23	STAB	Off
C14_CONV	64	62.5	69	50.0	14.4	0.23	CONV	Off
C14_SCT	64	62.5	69	50.0	14.4	0.23	STAB	On
E07	128	31.3	100	20.0	7.2	0.23	STAB	Off
F04	224	17.9	200	10.0	4.1	0.23	STAB	Off

added to the model θ equation above 1000 m, which ensured that the mean temperature profile gradient between 1000 m and the domain top remained constant [i.e., $\langle\theta\rangle_{z>1000\text{m}} = \langle\theta\rangle_{z=1000\text{m}} + 0.003(z - 1000\text{ m})$ at all times]. Temperatures below 1000 m were left to run free as normal. The effect of this procedure was to prevent the sharpening of the temperature gradients in the inversion region, which has been seen in other similar LES of the convective boundary layer (e.g., Mason 1989; Schmidt and Schumann 1989). It also inhibited the inversion rise so that the boundary layer depth (z_i) remained between 1000 and 1050 m in all cases. However, the entrainment fluxes remain very similar to those found in other studies [maximum downward heat fluxes at the inversion of size $(0.15 \pm 0.02)\langle w'\theta'\rangle_0$] and the influence of this modification on the turbulence statistics in the boundary layer interior is thought to be minimal.

Six different resolutions were employed. Grid A (the coarsest) has a spacing of 125 m in both horizontal directions. Grid B has this spacing reduced by a factor of $\sqrt{2}$, and each of grids C, D, and E shows a further reduction by the same factor. Finally, the highest-resolution grid, F, used a horizontal spacing $\sqrt{3}$ times smaller than that in grid E, giving a factor of 7 between the spacings in the finest and coarsest grids. In all cases the domain is 3000 m deep, with the damping layer above 2000 m. The vertical resolution was chosen so that throughout the boundary layer, it is always at least as good as that in the horizontal (although in the higher-resolution configurations it was degraded in the damping layer in order to save resources). Separate tests (not shown) indicated that the results are insensitive to the vertical spacing as long as this criterion is satisfied. Additionally, the grids are refined in the lowest third of the boundary layer so that the vertical resolution at the surface is typically at least a factor of 2 better than the horizontal resolution. Further tests indicated that the effects of this modification, which is desirable in principle in order to better capture ''squashing'' of large convective eddies close to surface, do not have an impact on the overall turbulence statistics that could be shown to be statistically significant.

A summary of the main runs performed can be found in Table 1. Here $N_{x,y}$ is the number of grid points in the horizontal directions, and $\Delta_{x,y}$ is the grid spacing in these directions. Similarly, N_z is the number of points in the vertical and Δ_z is the grid spacing in this direction throughout the middle and upper boundary layers. The basic length scale of the subgrid model is λ_0. Note that the naming convention is designed so that the resolution of each simulation (ranging from ''A'' for coarsest to ''F'' for finest) and the approximate value of λ_0 can be immediately ascertained. Here C_s is defined to be equal to $\lambda_0/\Delta_{x,y}$. No measure of the vertical resolution is included here, because the finding that increasing the vertical resolution with fixed horizontal resolution has minimal impact indicates that the effective grid resolution is being governed by the coarser horizontal spacing. ''STAB'' indicates that a simulation used the stability-dependent subgrid model of Brown et al. (1994), while ''CONV'' indicates that the conventional model was used (see previous section), and the final column indicates whether the stochastic backscatter parameterization was switched on. Additionally, the horizontal resolution and subgrid length scale of some of the main simulations are indicated in Fig. 2, in order to highlight the different comparisons that can be made (see below).

This choice of simulations was made in order to allow a number of different issues to be addressed. First of all, there is the question of domain size. In all cases bar one, the horizontal domain is a square of side 4000 m ($\simeq 4z_i$). Mason (1989) and Sykes and Henn (1989) suggested that such a domain is adequate, but the additional computing power now available allowed simulation C14_BIG to be run with a much larger domain ($\simeq 14z_i$), while retaining the credible horizontal resolution of simulation C14. The results of two simulations can therefore be compared to look at the impact of domain size.

Second, there is the issue of the independence of the filter and the numerical grid. Moving along the solid

Unauthenticated | Downloaded 07/25/21 03:39 AM UTC

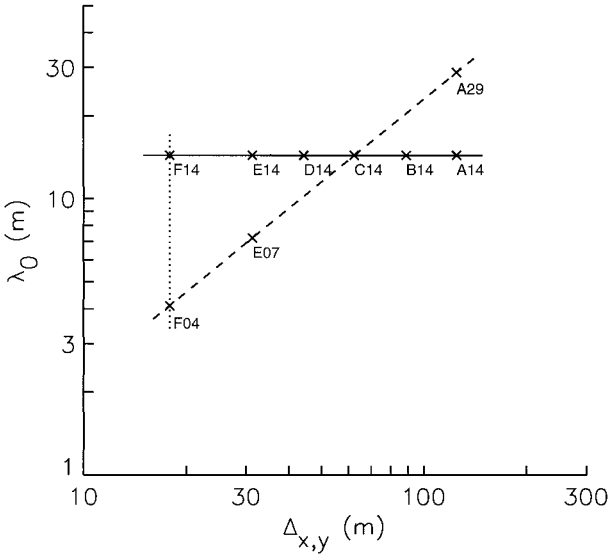

FIG. 2. Horizontal grid spacing ($\Delta_{x,y}$) and subgrid length scale (λ_0) of the main simulations. The solid line is $\lambda_0 = 14.4$ m, the dotted line is $\Delta_{x,y} = 17.9$ m, and the dashed line is $C_s = \lambda_0/\Delta_{x,y} = 0.23$.

line in Fig. 2 (simulations A14 through to F14) indicates the effect of changing resolution (and hence C_s) while keeping λ_0 constant. Thus, according to the arguments of Mason and Callen (1986), all are numerical solutions of the same set of continuous equations [(1)–(8)], and hence convergence of all aspects of the solutions (including spectra) should be expected as the resolution increases. In contrast the comparison of F04 and F14 (dotted line in Fig. 2) shows the effect of changing λ_0 (and C_s) at fixed resolution. If Mason and Callen are correct and the filter is determined by the subgrid model, then these simulations should resolve a different range of scales, even though their computational grids are identical.

Third, there is the issue of convergence of LES results with decreasing filter scale. Moving along the dashed line in Fig. 2 (comparison of simulations A29, C14, E07, and F04) shows the effects of changing resolution and subgrid length scale together, so that C_s stays constant ($=0.23$). This comparison cannot give information on whether the filter depends on the grid or on the subgrid length scale, as the two vary together. However, either way, the filter scale will depend on position on this line, and a different range of scales will be resolved in each simulation. Thus the level of convergence of the results (resolved plus subgrid estimates) of the three simulations can be regarded as a test of the subgrid model and of the reliability of the LES results.

Finally, the comparisons between A29 and C14 and A29_CONV and C14_CONV, and between C14 and C14_SCT, show the sensitivity of the results to the stability dependence of the subgrid model and to the use of stochastic backscatter.

All simulations were run for 10 000 s. Averages were collected over the last 4000 s in each case, a period that is equal to approximately $5t_*$, where t_* is the eddy turnover time ($=z_i/w_*$, where w_* is the convective velocity scale). Here $\langle\xi\rangle$ indicates an average of quantity ξ over this period and over the horizontal domain. The one-dimensional spectra presented in this study were taken in the x direction, and were averaged over the y direction and over time. Additionally, simulation C14 was run on for a further three averaging periods of 4000 s. Profiles and spectra shown from simulation C14 will be from the 6000- to 10 000-s averaging period, but additionally a shaded region will indicate the range of results obtained from the four consecutive averaging periods. Thus some insight can be gained into the statistical reliability of results obtained using a single 4000-s average. In most of the results presented statistical stability is not an important issue, as the differences between the results of the various runs will be shown to be larger than the differences between the various results from simulation C14, although it will be shown that this is not clearly the case for the velocity variance profiles (and low wavenumber spectra).

3. Results

a. Effects of domain size

The domain size test is considered first, as interpretation of all of the results would be complicated if domain size restrictions were found to be an important issue. Reassuringly, this is not the case. Simulations C14 and C14_BIG have the same grid spacing and value of λ_0, but C14_BIG has three-and-a-half times as many grid points in each of the horizontal directions and thus, given the same spacing, has a square domain of side $14z_i$ instead of $4z_i$. The total velocity variances $\langle u'u'\rangle$ and $\langle w'w'\rangle$ and the subgrid contribution to each $\langle 2E/3\rangle$ can be seen to be in extremely good agreement from these two simulations (Fig. 3a), with such differences as do exist being small compared to the statistical uncertainties associated with a single 4000-s average from simulation C14. Furthermore, the spectra are in excellent agreement across the range of wavenumbers captured by both simulations. See, for example, Fig. 3b, which shows one-dimensional spectra of vertical velocity at two heights in the boundary layer.

No further results will be shown from simulation C14_BIG, as in none of the statistics examined have the differences from the results of simulation C14 appeared to be significant. Instead the main results concerning the independence of the filter and grid, and the convergence of results with decreasing filter scale will now be presented.

b. Convergence and the independence of filter and grid

Figures 4–8 show statistics from some of the simulations. They are one-dimensional spectra of the w com-

Unauthenticated | Downloaded 07/25/21 03:39 AM UTC

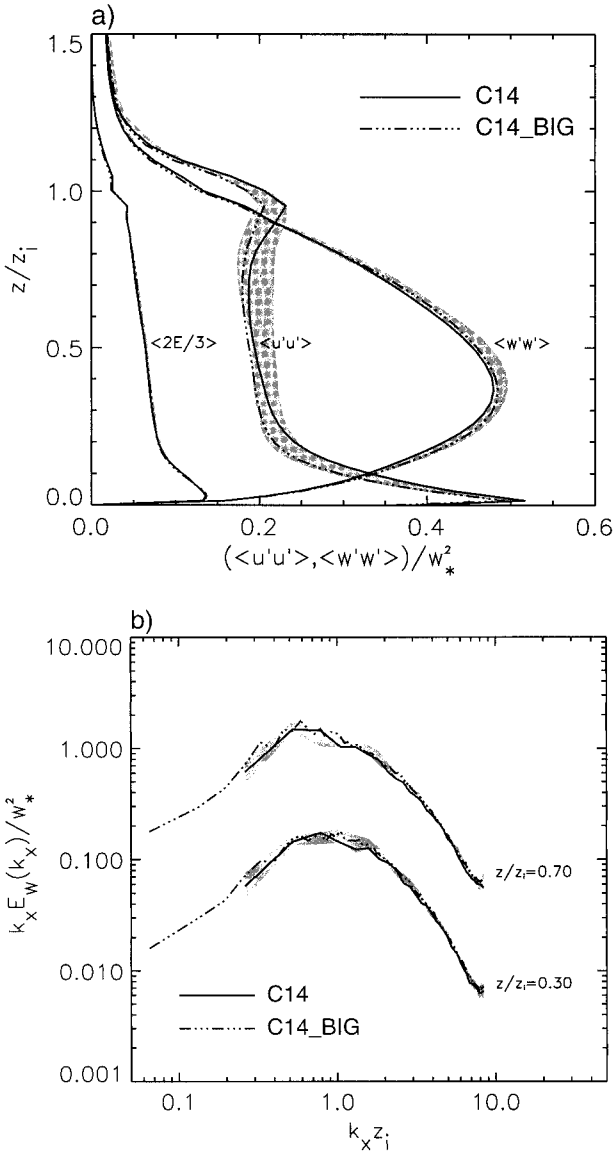

FIG. 3. Results from simulations C14 and C14_BIG. The shaded regions show the range of results obtained in four successive averaging periods of 4000 s from simulation C14. (a) Profiles of total (resolved plus subgrid) horizontal and vertical velocity variance, and the subgrid contribution to these variances ($\langle 2E/3 \rangle$); (b) normalized one-dimensional vertical velocity spectra at $z/z_i = 0.30$ and $z/z_i = 0.70$. The spectra have been taken in the x direction, and k_x is the wavenumber (=1/wavelength). Note that for clarity the spectral estimates at $z/z_i = 0.70$ have been multiplied by 10.

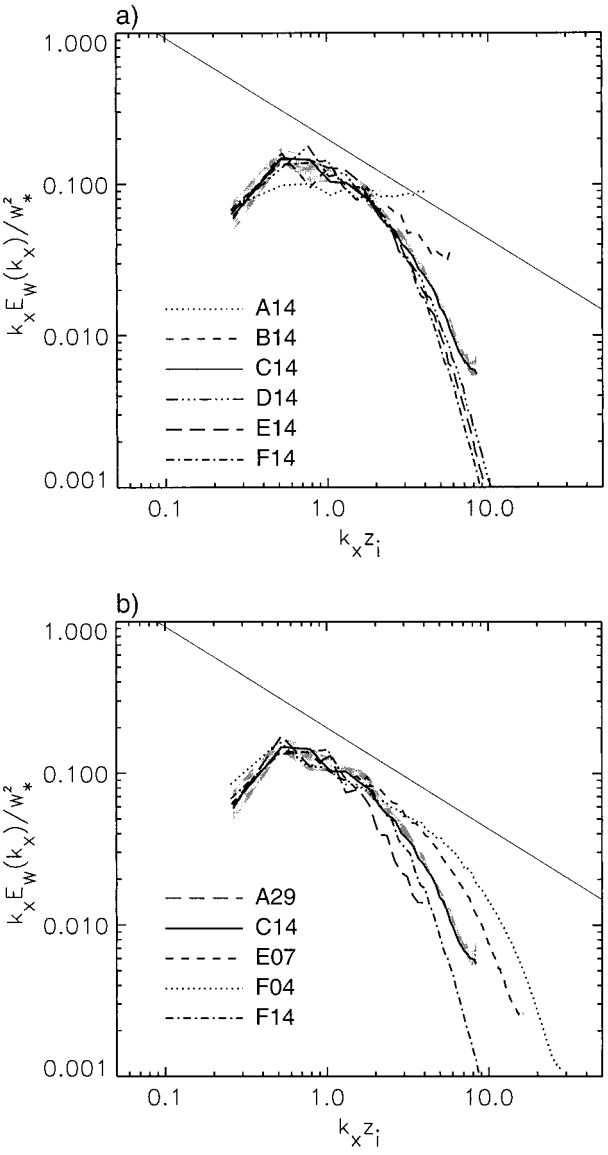

FIG. 4. Normalized one-dimensional w spectra at $z/z_i = 0.7$. (a) Simulations A14, B14, C14, D14, E14, and F14; (b) simulations A29, C14, E07, F04, and F14; shaded regions as in Fig. 3.

ponent of velocity at $z/z_i = 0.7$ (Fig. 4); one-dimensional spectra of the v component at the same height (Fig. 5); profiles of total horizontal and vertical velocity variance and $2E/3$, the subgrid contribution to these variances (Fig. 6); and profiles of $\langle w'w'w' \rangle / \langle w'w' \rangle^{3/2}$, the vertical velocity skewness (Fig. 7). Following Mason (1989), total $\langle w'w'w' \rangle$ is estimated by adding two-thirds of $\langle w'E \rangle$ to the resolved value. The entirely subgrid-scale contribution to $\langle w'w'w' \rangle$ is neglected but is not expected to be significant in the flow interior.

In each figure, panel (a) shows results from simulations A14, B14, C14, D14, E14, and F14 and thus shows the effect of changing resolution with fixed subgrid length scale. Panel (b) shows results from A29, B14, E07, and F04 and therefore indicates the effect of changing resolution and length scale together (with fixed C_s). Additionally, each panel (b) shows results from F14, thus allowing comparison of F04 and F14, which have the same resolution but different subgrid length scale. Discussion of the results is split into two sections, first demonstrating the independence of the filter and the

Unauthenticated | Downloaded 07/25/21 03:39 AM UTC

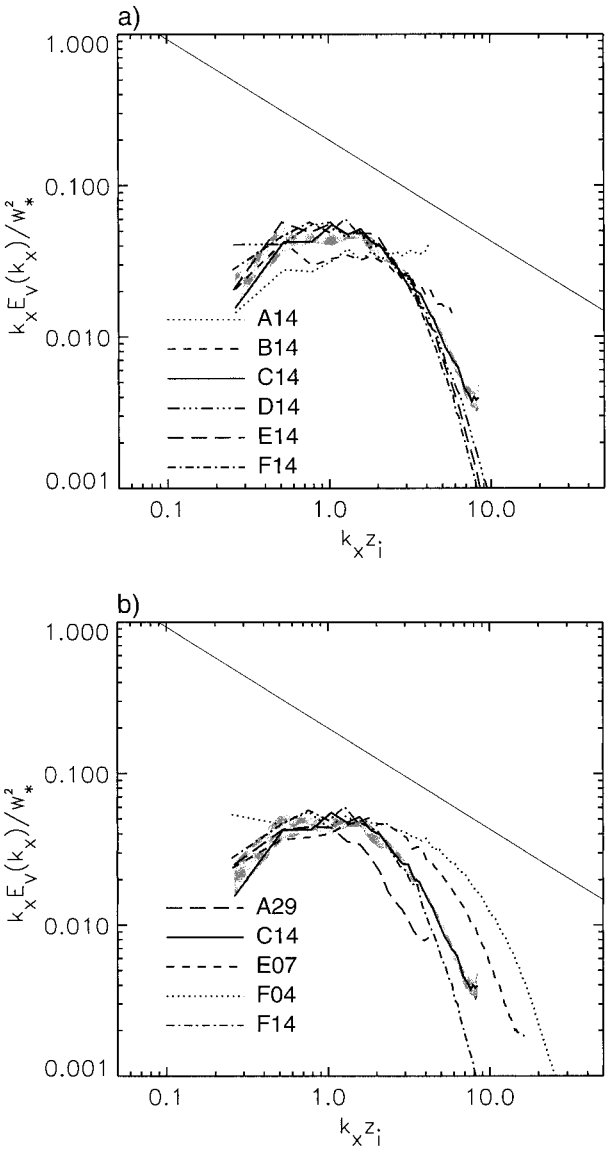

FIG. 5. Normalized one-dimensional v spectra at $z/z_i = 0.7$. (a) Simulations A14, B14, C14, D14, E14, and F14; (b) simulations A29, C14, E07, F04, and F14; shaded regions as in Fig. 3.

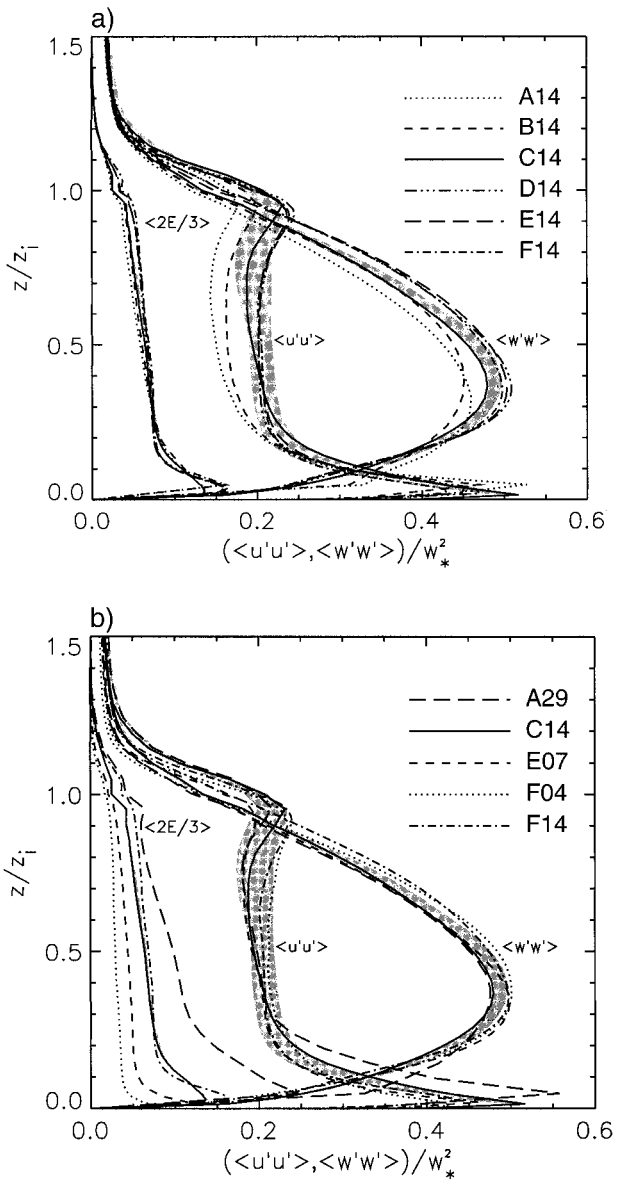

FIG. 6. Profiles of total horizontal and vertical velocity variances, and the subgrid contribution to these variances. (a) Simulations A14, B14, C14, D14, E14, and F14; (b) simulations A29, C14, E07, F04, and F14; shaded regions as in Fig. 3.

numerical grid and then looking at the convergence of the results with decreasing filter scale.

1) INDEPENDENCE OF FILTER AND GRID

Figures 4a and 5a show vertical and horizontal velocity spectra at $z/z_i = 0.7$ from the six simulations with constant λ_0 but varying grid resolution. Both show convincing evidence for convergence of the results with increasing resolution, as the differences between the results from the higher-resolution simulations (D14, E14, and F14) are much smaller than the differences between those from the lower-resolution simulations (A14, B14, and C14). Thus it seems likely that the highest-resolution simulation, F14, which has $C_s = 0.81$, gives an answer close to that which would be obtained in the continuous limit ($C_s \to \infty$). Simulations E14 ($C_s = 0.46$), D14 ($C_s = 0.32$), and, to lesser extent, C14 ($C_s = 0.23$) give very similar solutions. This convergence is consistent with the filter being determined by the subgrid model rather than by the numerical grid, as these simulations show a wide variation in resolution and yet resolve the same range of scales.

Similar convergence has been found in all of the statistics examined. See, for example, the velocity variance profiles in Fig. 6a and the vertical velocity skewness

Unauthenticated | Downloaded 07/25/21 03:39 AM UTC

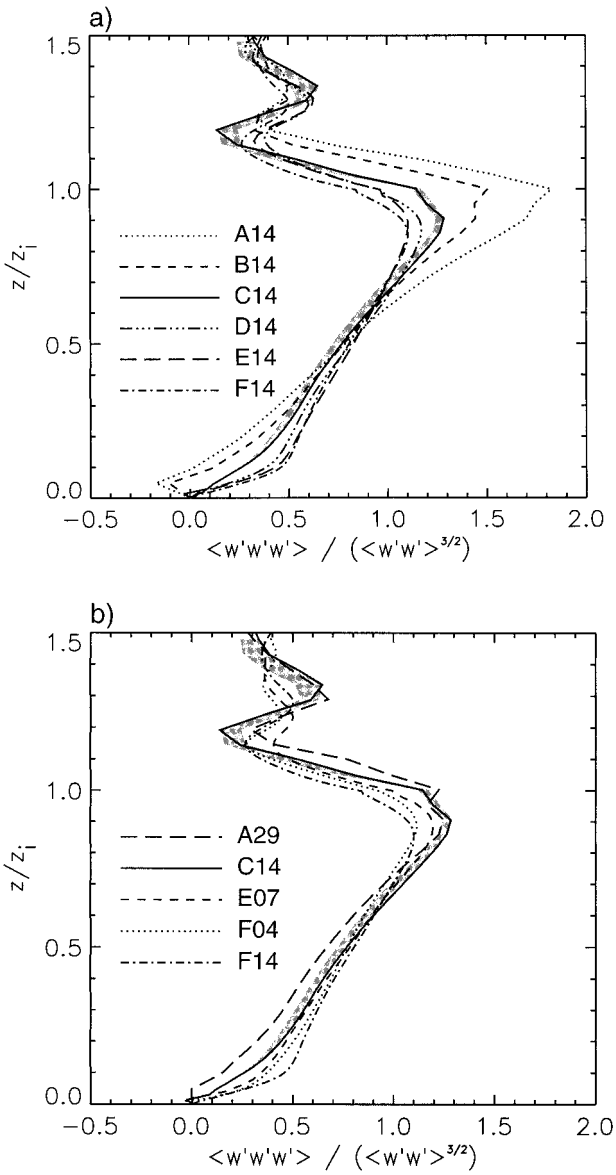

FIG. 7. Profiles of vertical velocity skewness, $\langle w'w'w'\rangle/(\langle w'w'\rangle)^{1.5}$. (a) Simulations A14, B14, C14, D14, E14, and F14; (b) simulations A29, C14, E07, F04, and F14; shaded regions as in Fig. 3.

profiles in Fig. 7a. The three solutions with $C_s \geq 0.32$ give very similar results, and the solution obtained using $C_s = 0.23$ may be adequate for most practical purposes. However, the lower-resolution grids used in B14 ($C_s = 0.16$) and A14 ($C_s = 0.12$) do give less satisfactory solutions, and they appear to be insufficiently fine to properly represent the filter given by the Smagorinsky model with $\lambda_0 = 14$ m; the grid starts to have an influence. Both show a significant loss (relative to the higher-resolution simulations) of horizontal and vertical velocity variance throughout most of the boundary layer, and the negative skewness values close to the surface are also indicative of finite difference errors. The spectra show a loss of energy at small wavenumbers, and a failure to resolve a steep spectral falloff at high wavenumbers. Thus, although the spectra from B14 are close to following a $-\frac{2}{3}$ slope at the smallest scales (as expected in an inertial subrange), this is not regarded as evidence for success of this simulation, as there is evidence for significant contamination by finite difference errors.

Finally it is noted that the comparison of the spectra from simulations F04 and F14 (Figs. 4b and 5b) is also consistent with the filter being determined by the subgrid model rather than by the grid. Even though the grids used in the two simulations are identical, F04 resolves a wider range of scales, with the sharp falloff in spectral energy occurring at higher wavenumbers, due to its reduced value of λ_0.

2) CONVERGENCE OF RESULTS WITH DECREASING FILTER SCALE

Vertical velocity spectra at $z/z_i = 0.7$ from simulations A29, C14, E07, and F04 are shown in Fig. 4b. The thin solid line shows the $-\frac{2}{3}$ slope that is expected in an inertial subrange. The spectrum from simulation F04, which has the highest resolution and the smallest value of λ_0, appears to follow this slope over at a range of at least half a decade of wavenumbers before falling off more steeply. The spectra from simulations E07, C14, and A29 are encouragingly similar to that from simulation F04 at low wavenumbers, with the differences between them probably not statistically significant judging by the differences between the spectra obtained from the successive averaging periods of simulation C14. The wavenumbers at which the spectra start to fall off more steeply appear to be approximately inversely proportional to λ_0, which is consistent with the filter scale l_f being determined by λ_0. The horizontal velocity spectra (Fig. 5b) show a similar change in the range of scales resolved as λ_0 is reduced.

Figure 6b shows the profiles of total horizontal and vertical velocity variance from these simulations, and the subgrid contribution to these variances. As expected, the subgrid estimates are sensitive to filter scale; simulation A29 shows larger values of subgrid energy than simulation C14, which in turn shows larger values than E07 and F04. Nevertheless, the collapse of the total variance profiles in middle and upper boundary layers is reasonably convincing, particularly as no attempt has been made either to tune the subgrid energy estimate, or to partition that energy unevenly between the horizontal and vertical variances. There is a suggestion of a trend to slightly larger values of $\langle w'w'\rangle$ in mid–boundary layer as the filter scale (l_f) decreases, but the differences between the profiles from the different runs are comparable in size to those between successive averaging periods of simulation C14 and so longer averages would be required to show that these effects are more than statistical. In any event, the degree of convergence

Unauthenticated | Downloaded 07/25/21 03:39 AM UTC

is certainly far in excess of that found by Mason (1989). This is probably largely due to the change in the range of filter scales that could be examined in the two studies—Mason compared runs with λ_0 equal to 92, 46, and 23 m, and so even the best resolved run in that study was only slightly better resolved than the poorest one in this. It is also conceivable that the change to the stability-dependent subgrid model of Brown et al. (1994) might have led to improved convergence of the results, but the tests to assess this prove inconclusive; horizontal and vertical velocity variance profiles (not shown) from the simulations using the conventional subgrid model, A29_CONV and C14_CONV, show values slightly smaller [by $O(0.02w_*^2]$ in mid–boundary layer than the corresponding simulations, A29 and C14. Assuming that these changes are more than statistical fluctuations (which could only be confirmed by extending the averaging period), it can be noted that the results with the conventional model are further from those of the best resolved simulation, F04, and so, if it is assumed that all models should converge to the same limit as the filter scale reduces, this could be regarded as evidence that the conventional model converges less quickly. However, as the conventional and stability-dependent subgrid models behave differently in the near-surface region (see next section), it is not clear that the two models should be expected to give the same limiting result, as there will always be some height at which the simulation is poorly resolved and where the differences between the subgrid models are important.

The scalar variance profiles (not shown) also collapse reasonably convincingly. However, the skewness involves a third-order moment, and the vertical velocity skewness profiles (Fig. 7b) from simulations A29, C14, E07, and F04 do show small, but apparently statistically significant differences, with a trend to larger values near the surface as λ_0 decreases. It is interesting that the differences between C14 and F14 appear to be larger than those between C14 and F04. This suggests that, in order to obtain more robust results for third-order moments, at least some of any further increase in available computing resources should be put toward reducing finite difference errors by using larger values of C_s (e.g., 0.32), rather than being entirely concentrated on decreasing filter scale at fixed $C_s = 0.23$.

The turbulence kinetic energy budgets from A29, C14, E07, and F04 also look similar, but there are some differences in the details. For example, Fig. 8 shows the total dissipation, which is equal to the sum of the dissipation from the resolved scales and the subgrid buoyancy flux. The vertical integral of this quantity varies only slightly (±2%) between the five cases shown (which must be the case as the buoyancy flux profiles collapse almost exactly). However, the profiles show a tendency for slightly increased dissipation in the boundary layer interior and much reduced dissipation close to the surface as the filter scale is reduced and transport of energy out of the surface layer is better captured.

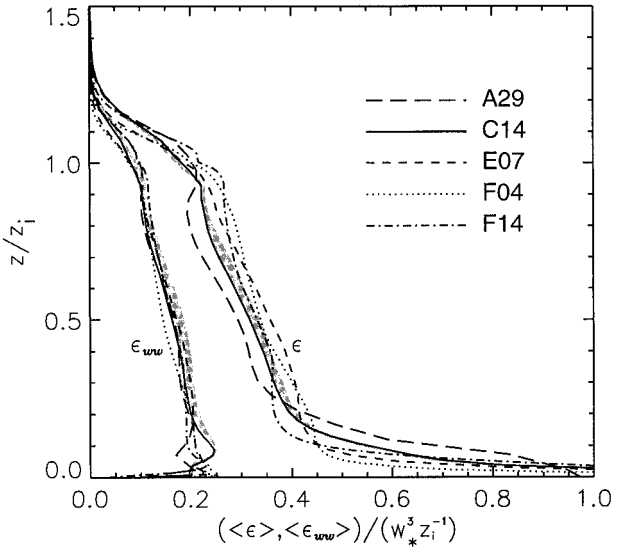

FIG. 8. Profiles of total dissipation (ϵ) and dissipation from $0.5\langle w'w'\rangle$ (ϵ_{ww}) from simulations A29, C14, E07, F04, and F14; shaded regions as in Fig. 3.

This lack of convergence close to the surface suggests that the details of the balance between production, dissipation, and transport in the lowest few model levels of any given simulation are probably spurious and should not be interpreted physically.

It is also noteworthy that although the convergence of the results in mid–boundary layer is generally satisfactory, and although the vertical velocity spectra from simulation F04 in particular appear to show a clear $-\frac{2}{3}$ slope (Fig. 4b), the spectra of the v component from this simulation appear to be only just beginning to show a range with a $-\frac{2}{3}$ slope (Fig. 5b). Hence, even this very high-resolution simulation is probably just starting to resolve into the inertial range, and at $k_x z_i = 5$ (where by eye the spectra were judged to start falling off more quickly) the w-, v-, and u-component spectral estimates are in the ratio 1.8:1.5:1.0. This appears to be slightly more isotropic than the $160 \times 160 \times 48$ simulation of Schmidt and Schumann (1989), and much more isotropic than the much lower-resolution simulations of Deardorff (1972), but further reductions in filter scale and a correspondingly longer inertial range would be required to get close to the ratio of 1.3:1.3:1.0 that is predicted by isotropy (Kaimal et al. 1972). As expected, the spectral ratios from the less well-resolved simulations are further from the inertial subrange result. For example, B14 gives around 3.7:1.6:1.0 at the shortest resolved scales. This suggests that the approximately $-\frac{2}{3}$ slope, which is maintained to the highest wavenumbers in this simulation ($C_s = 0.16$), does not truly indicate a well-resolved inertial subrange and is probably caused by a buildup of finite difference errors.

Similarly, in none of the simulations performed is the dissipation isotropic. Here ϵ is defined to be equal to the total dissipation rate $[=\langle \nu S^2(1 - Rf_p)\rangle]$, and ϵ_{ww} is

Unauthenticated | Downloaded 07/25/21 03:39 AM UTC

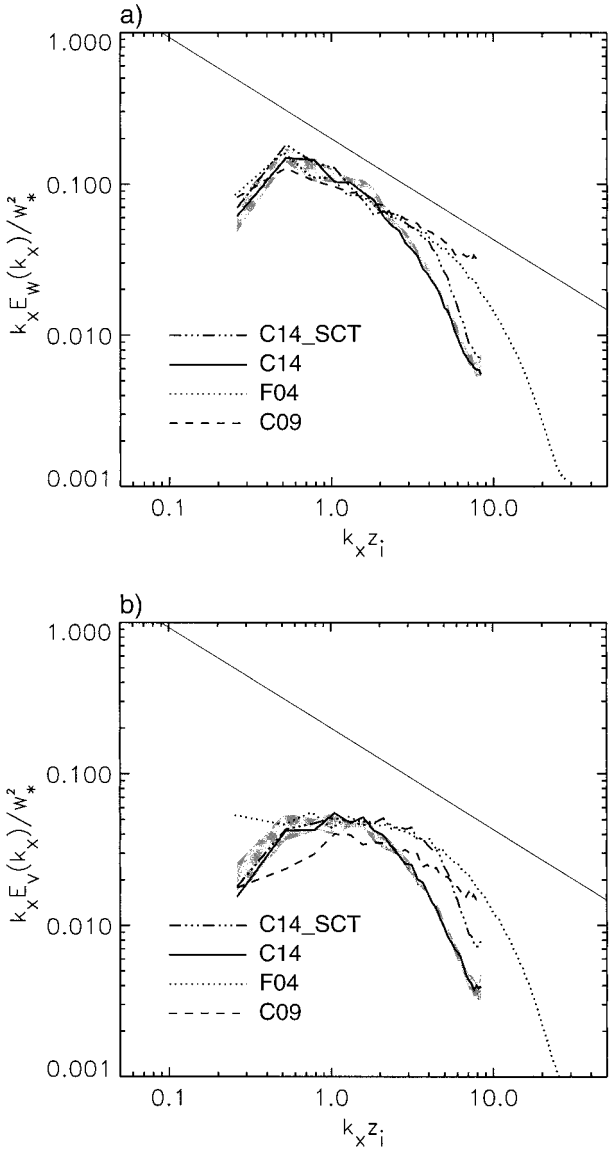

FIG. 9. Normalized one-dimensional velocity spectra at $z/z_i = 0.7$ from simulations C14_SCT, C14, F04, and C09. (a) w spectra; (b) v spectra; shaded regions as in Fig. 3.

half of the dissipation rate of the resolved vertical velocity variance. Both have been calculated in a manner exactly consistent with the finite difference representation in the model. The profiles in Fig. 8 show that ϵ_{ww} appears to be almost independent of filter scale, but because of the changes in total dissipation, it does account for a decreasing fraction of the total dissipation as the filter scale reduces, from between 50% and 60% in simulation A29 to around 40% in simulation F04. Again, further reductions in filter scale would presumably reduce this still further toward the expected value of 33%. Nevertheless, the lack of a long well-resolved inertial range even in this very high-resolution simulation suggests that, particularly at lower resolution, the use of a subgrid model that attempted to impose inertial range results (e.g., spectral slope), or the assessment of the merits of a model based on whether it reproduced those results, might be misguided. It is noted that a dynamic model, with numerical grid B, might tend to give results similar to those seen in simulation B14 ($C_s = 0.16$) and, hence, might be prone to finite difference errors.

c. The effect of stochastic backscatter

As expected, the impact of stochastic backscatter is found to be small. The velocity variance, temperature variance, and skewness profiles from simulation C14_SCT (not shown) all lie slightly closer to the results of the high-resolution simulation F04 than do those from the same averaging period of simulation C14. However, the changes lie within the spread of values from the four successive averaging periods of C14 and so, while encouraging, this can be no more than a suggestion of improved performance at moderate resolution when using backscatter.

The one clearly statistically significant change associated with the use of backscatter is in the shape of the high-wavenumber spectra. Figure 9 shows the w and v spectra from simulation C14_SCT and those from C14 and F04. The effect of backscatter (C14_SCT compared to C14) is clearly to make the steep falloff occur at higher wavenumbers, with the spectra from the simulation using backscatter following those from the high-resolution simulation (F04) over a greater range of wavenumbers than those from the simulation using the standard Smagorinsky model. Furthermore, the increase in high-wavenumber energy is more marked in the horizontal component. Encouragingly this makes the distribution of the turbulence kinetic energy more isotropic at the new point where the steep spectral falloff occurs ($k_x z_i \cong 4$). It is also noted that the falloff is slightly steeper than in the nonbackscatter run.

Mason and Thomson (1992) extended the analysis of Lilly (1967) to include backscatter and concluded that, for fixed λ_0, the backscatter model causes a reduction in the filter scale l_f relative to that of the Smagorinsky model. Specifically, in neutral conditions at least, their analysis suggests that l_f changes to $l_f/1.55$. This is consistent with the effect of backscatter shown in Fig. 7, but the process is having a more subtle effect than can be reproduced simply by changing λ_0. To show this, an additional simulation (C09) was performed using the same grid as C14_SCT, but without backscatter and with the basic length scale reduced by a factor of 1.5 (giving $\lambda_0 = 9.4$ m, $C_s = 0.15$). The spectra from C09 (also shown on Fig. 9) fail to show the same steep spectral falloff before the grid scale, and this simulation appears to have been adversely affected by finite difference errors.

Unauthenticated | Downloaded 07/25/21 03:39 AM UTC

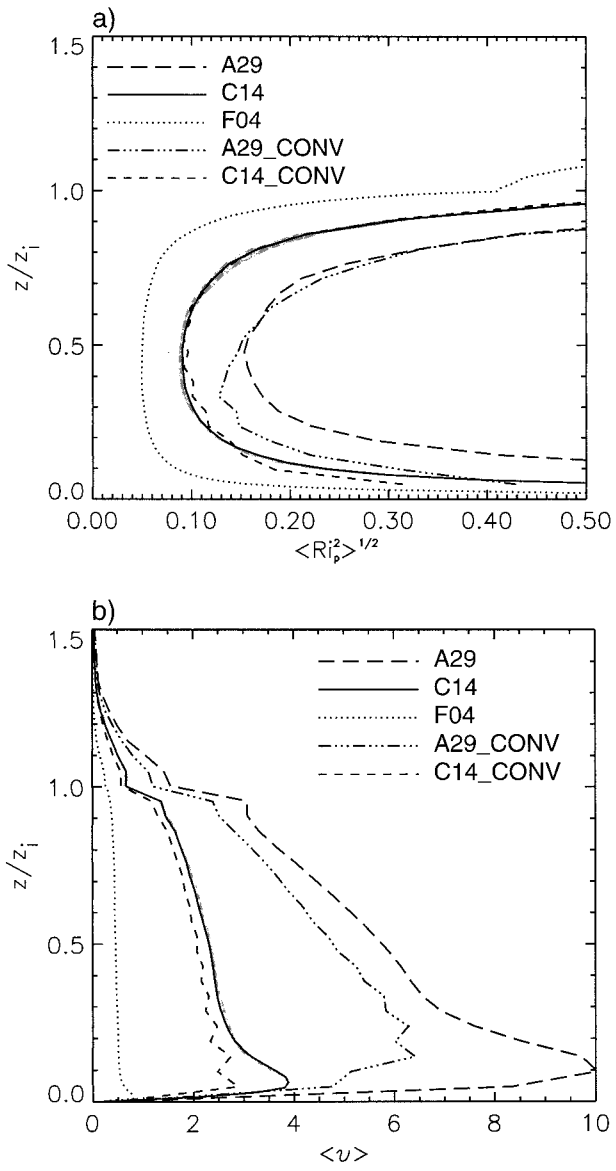

FIG. 10. Profiles from simulations A29, C14, F04, A29_CONV, and C14_CONV. (a) Root-mean-square pointwise Richardson number; (b) viscosity; shaded regions as in Fig. 3.

d. Near-surface behavior of the subgrid model

In a well-resolved inertial subrange, the pointwise Richardson number Ri_p should be close to zero, and the stability dependence of the subgrid model unimportant. Figure 10a shows profiles of root-mean-square Ri_p, and it can be seen that the values in the boundary layer interior do decrease monotonically as the filter scale reduces (simulations A29, C14, and F04). However, all of the simulations show a large increase in Ri_p as the surface is approached and the turbulence becomes less well resolved. Improving resolution reduces the height above the surface at which this occurs but cannot remove the effect, and the stability dependence of the subgrid model will always become important at some point. Of course, the values of Ri_p depend on the turbulent fields, which themselves are affected by that stability dependence, but the profiles from the simulations using the conventional model (A29_CONV and C14_CONV) show the same features as those from the model of Brown et al. (1994) (A29 and C14), although the sharp increases occur slightly closer to the surface.

The averaged viscosity profiles from the same five simulations are shown in Fig. 10b. The values from simulation F04 are considerably smaller than those from C14, which in turn are small compared to those from A29. This is primarily due to the changes in the basic length scale λ_0, although the peaks close to the surface are related to stability effects; as the simulations become less well resolved close to the surface, Ri_p tends to become more negative (Fig. 10a) and the subgrid model increases the viscosity above its neutral value. The simulations using the conventional subgrid model show similar behavior in the boundary layer interior where stability effects are comparatively unimportant (although not completely negligible, especially in the lowest-resolution simulations), but have much smaller viscosities close to the surface. The impact of this change on the spectral behavior in the near-surface region is now examined.

Figure 11 shows one-dimensional vertical velocity spectra at various heights below $z/z_i = 0.3$ from simulations C14, C14_CONV, F04, and F14. Note that while the spectra have been averaged in the y direction (as before), no time averaging has been applied. This makes the spectra rather more noisy (e.g., cf. the simulation C14 results at $z/z_i = 0.3$ in Fig. 11a, which have not been time averaged, with those in Fig. 3b, which have) but does not significantly change the spectral shape. Figure 11a indicates that the stability-dependent subgrid model is successful in preventing a buildup of energy at small scales close to the surface, and the results are consistent with the filter scale implied by the subgrid model being independent of height. Similar behavior is found for the high-resolution runs, both with $C_s = 0.23$ (simulation F04, Fig. 11b) and with $C_s = 0.81$ (simulation F14, Fig. 11c). The backscatter run C14_SCT also shows this satisfactory behavior (not shown). In contrast, simulation C14_CONV (Fig. 11d) shows an undesirable buildup of energy at, and close to, the grid scale as the surface is approached. This is consistent with the smaller values of viscosity found when using this only weakly stability-dependent subgrid model (Fig. 10b).

4. Conclusions

The main conclusions of this paper should be relevant to the application of any subgrid model in large eddy simulations. Furthermore, related arguments apply in a wider range of numerical simulations with closures or parameterizations of some form (Lander and Hoskins

Unauthenticated | Downloaded 07/25/21 03:39 AM UTC

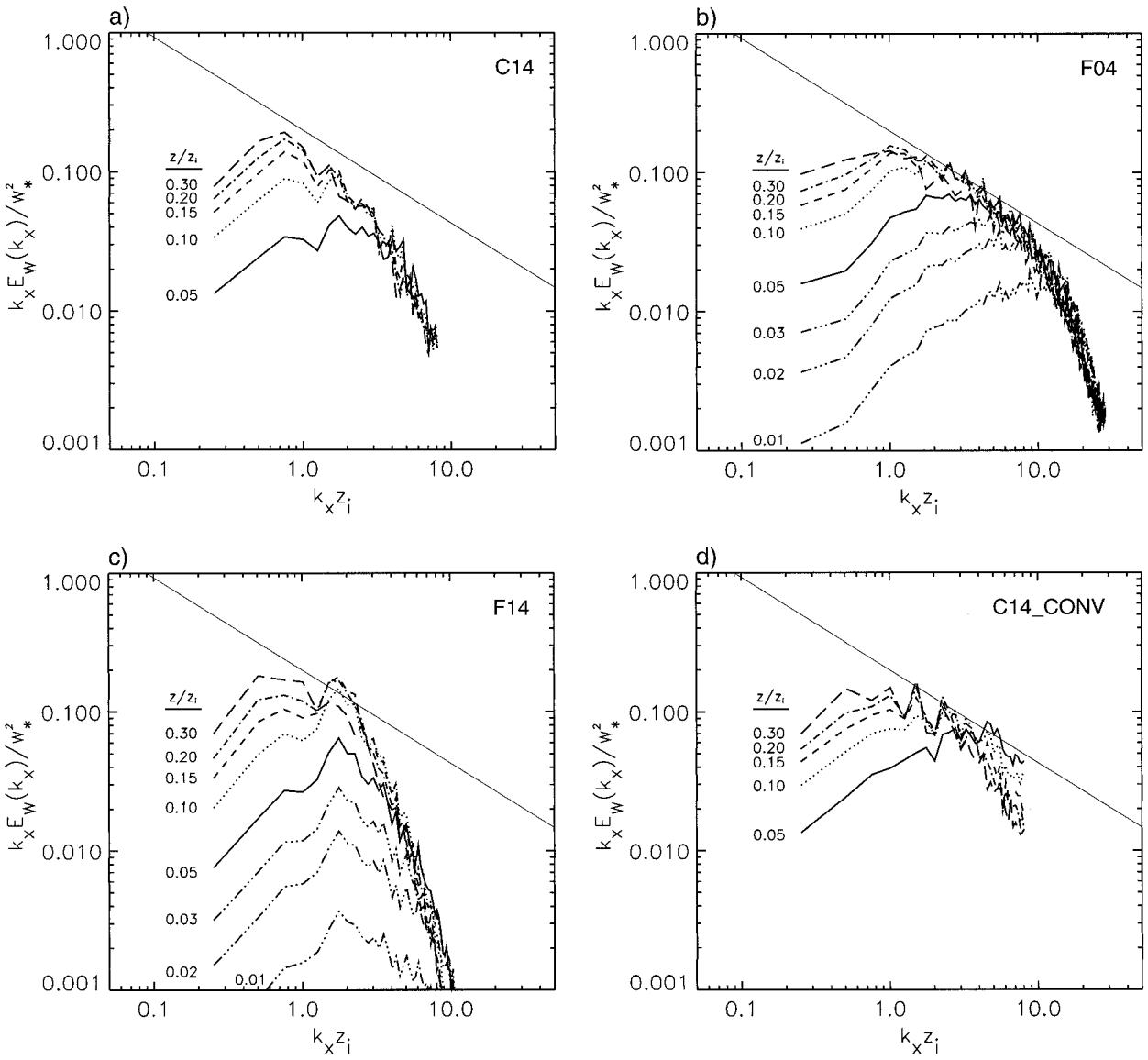

FIG. 11. Normalized one-dimensional (instantaneous) spectra of vertical velocity at various heights (for $z/z_i \leq 0.3$). (a) C14; (b) F04; (c) F14; (d) C14_CONV.

1997). From the large eddy simulation spectral behavior and flow statistics it has been shown that the subgrid model determines the filter operation (and would better be called the subfilter model in order to emphasize its independence from the numerical grid). Ideally the numerical resolution should be sufficient to allow good resolution of this filter. The constant of the Smagorinsky model C_s is a measure of the ratio of this filter scale to the numerical resolution. In practice, a solution using the Smagorinsky subgrid model with a value of C_s less than about 0.23 showed divergence from the correct solution as judged by higher C_s simulations with higher numerical resolution but the same filter operation. The results obtained with $C_s = 0.23$ and 0.81 (still with fixed filter operation) were broadly similar, although use of $C_s = 0.32$ appeared to be marginally beneficial, particularly for the third-order moments. Values of C_s larger than about 0.32 are helpful to clarify the role of finite difference errors in other simulations but, in terms of the most efficient use of computer resources, are not generally recommended.

A subsidiary general result concerns the presence of inertial subrange behavior in current large eddy simulations. As a consequence of the large scale of convective turbulence, an inertial subrange ought to be most accessible in such flows. Here it is noted that in the highest-resolution simulation with $C_s = 0.23$ (which ought to fairly represent the filter operation), a characteristic slope of $-\frac{2}{3}$ in the spectral energy density can be discerned over only a limited range of scales. Fur-

Unauthenticated | Downloaded 07/25/21 03:39 AM UTC

thermore, the distribution of the energy between and the dissipation from the three components are not in good agreement with the expected values, and strict inertial subrange interpretation would be unwise. Values of C_s lower than 0.23 allow an apparently correct spectral shape to occur at the smallest scales represented on the numerical grid but, as noted, such solutions are in fact inferior with a degradation being apparent in other aspects of the flow statistics.

The more detailed conclusions relate to the use of the Smagorinsky type of model in buoyant flows. It is found desirable, in terms of consistent spectral behavior, to adopt a subgrid model buoyancy dependence based on observations of the atmospheric surface layer. This was achieved using the model proposed by Brown et al. (1994) and involves both the subgrid energy and the subgrid length scale being buoyancy dependent. In these well-resolved flows, the further refinement of the subgrid model to include backscatter proved to be a minor influence, giving some improvement in spectral behavior and the suggestion of slight but general improvement in turbulence statistics, in the sense of results closer to those obtained in higher-resolution simulations with smaller filter scales. In achieving these results the present work has made a number of state-of-the-art simulations of the convective planetary boundary layer. The results show some of these statistics but the full set are available from the authors on request.

This study has shown that the view of a filter operation being specified by the subgrid model is valid. It has further illustrated that appropriate buoyancy dependence in the subgrid model can lead to the filter operation being nearly independent of buoyant instability. It remains for future studies to see whether any subgrid model can specify a filter operation that is also invariant to shear and stable stratification. Past studies suggest that backscatter may play an important role in such cases. It is also possible (e.g., Canuto and Cheng 1997) that the presence of mean shear itself may be a significant influence.

APPENDIX

Stability Dependence of the Subgrid Model

The stability functions, f_m and f_h, used in the subgrid model of Brown et al. (1994) are given here for ease of reference.

In neutral and unstable conditions ($\mathrm{Ri}_p \leq 0$) the model uses

$$f_{um} = (1 - 16\mathrm{Ri}_p)^{0.5} \tag{A1}$$

and

$$f_{uh} = 1.43(1 - 40\mathrm{Ri}_p)^{0.5}. \tag{A2}$$

In statically stable conditions, with the pointwise Richardson number less than the critical value ($\mathrm{Ri}_c = 0.25$), the stability functions are given by

$$f_{sm} = \left(1 - \frac{\mathrm{Ri}_p}{\mathrm{Ri}_c}\right)^4 \tag{A3}$$

and

$$f_{sh} = 1.43\left(1 - \frac{\mathrm{Ri}_p}{\mathrm{Ri}_c}\right)^4 (1 - 1.2\mathrm{Ri}_p), \tag{A4}$$

and both f_{sm} and f_{sh} are set to zero for $\mathrm{Ri}_p > \mathrm{Ri}_c$.

REFERENCES

Brown, A. R., S. H. Derbyshire, and P. J. Mason, 1994: Large-eddy simulation of stable atmospheric boundary layers with a revised stochastic subgrid model. *Quart. J. Roy. Meteor. Soc.,* **120,** 1485–1512.

Canuto, V. M., and Y. Cheng, 1997: Determination of the Smagorinsky–Lilly constant C_s. *Phys. Fluids,* **9,** 1368–1378.

Deardorff, J. W., 1972: Numerical investigation of neutral and unstable planetary boundary layers. *J. Atmos. Sci.,* **29,** 91–115.

Germano, M., U. Piomelli, P. Moin, and W. H. Cabot, 1991: A dynamic subgrid-scale eddy viscosity model. *Phys. Fluids,* **A3,** 1760–1765.

Kaimal, J. C., J. C. Wyngaard, Y. Izumi, and O. R. Coté, 1972: Spectral characteristics of surface-layer turbulence. *Quart. J. Roy. Meteor. Soc.,* **98,** 563–589.

Lander, J., and B. J. Hoskins, 1997: Believable scales and parametrizations in a spectral transform model. *Mon. Wea. Rev.,* **125,** 292–303.

Leonard, A., 1974: Energy cascade in large-eddy simulations of turbulent fluid flows. *Advances in Geophysics,* Vol. 18, Academic Press, 237–248.

Lilly, D. K., 1962: On the numerical simulation of buoyant convection. *Tellus,* **14,** 148–171.

——, 1967: The representation of small-scale turbulence in numerical simulation experiments. *Proc. 10th Scientific Computing Symp. on Environmental Sciences,* Yorktown Heights, NY, IBM, 195–210.

Mason, P. J., 1989: Large-eddy simulation of the convective atmospheric boundary layer. *J. Atmos. Sci.,* **46,** 1492–1516.

——, and N. S. Callen, 1986: On the magnitude of the subgrid-scale eddy coefficient in large-eddy simulations of turbulent channel flow. *J. Fluid Mech.,* **162,** 439–462.

——, and D. J. Thomson, 1992: Stochastic backscatter in large-eddy simulations of boundary layers. *J. Fluid Mech.,* **242,** 51–78.

——, and A. R. Brown, 1994: The sensitivity of large-eddy simulations of turbulent shear flow to subgrid models. *Bound.-Layer Meteor.,* **70,** 133–150.

Moeng, C.-H., and J. C. Wyngaard, 1988: Spectral analysis of large-eddy simulations of the convective boundary layer. *J. Atmos. Sci.,* **45,** 3573–3587.

Muschinski, A., 1996: A similarity theory of locally homogeneous and isotropic turbulence generated by a Smagorinsky-type LES. *J. Fluid Mech.,* **325,** 239–260.

Piacsek, S. A., and G. P. Williams, 1970: Conservation properties of convection difference schemes. *J. Comput. Phys.,* **6,** 392–405.

Schmidt, H., and U. Schumann, 1989: Coherent structure of the convective boundary layer derived from large-eddy simulation. *J. Fluid Mech.,* **200,** 511–562.

Schumann, U., 1995: Stochastic backscatter of turbulence energy and scalar variance by random subgrid-scale fluxes. *Proc. Roy. Soc. London,* **A451,** 293–318.

Smagorinsky, J., 1963: General circulation experiments with the primitive equations. I. The basic experiment. *Mon. Wea. Rev.,* **91,** 99–164.

Sykes, R. I., and D. S. Henn, 1989: Large-eddy simulation of turbulent sheared convection. *J. Atmos. Sci.,* **46,** 1106–1118.

Unauthenticated | Downloaded 07/25/21 03:39 AM UTC